

Supporting Information for

Evidence for Low-pressure Crustal Anatexis During the Northeast Atlantic Break-up

A.M. Morris¹, S. Lambart¹, M.A. Stearns², J.R. Bowman¹, M.T. Jones³, G.T.F. Mohn⁴, G. Andrews⁵, J. Millet^{6,7}, C. Tegner⁸, S. Chatterjee⁹, J. Frieling¹⁰, P. Guo¹¹, D.W. Jolley⁶, E. H. Cunningham¹, C. Berndt¹², S. Planke^{3,7}, C.A., Alvarez Zarikian¹³, P. Betlem^{3,14}, H. Brinkhuis¹⁵, M. Christopoulou¹⁶, E. Ferre¹⁷, I.Y. Filina¹⁸, D. Harper¹, J. Longman¹⁹, R.P. Scherer¹⁶, N. Varela²⁰, W. Xu²¹, S.L. Yager²², A. Agarwal²³, V.J. Clementi²⁴

¹Geology & Geophysics Department, University of Utah, Salt Lake City, UT, USA; ²Department of Earth Sciences, Utah Valley University, Orem, UT, USA; ³Department of Ecology and Environmental Science, Umeå University, Umeå, Sweden; ⁴Laboratoire Géosciences et Environnement Cergy, University of Cergy-Pontoise, Cergy, France; ⁵School of Environmental Sciences, University of Hull, Hull, UK; ⁶Department of Geology and Geophysics, University of Aberdeen, King's College, Aberdeen, UK; ⁷Volcanic Basin Energy Research AS, Høienhold, Oslo, Norway; ⁸Department of Geoscience, Aarhus University, Aarhus, Denmark; ⁹Earthquake Research Institute, The University of Tokyo, Bunkyo, Tokyo, Japan; ¹⁰Department of Earth Sciences, The University of Oxford, Oxford, UK; ¹¹Institute of Oceanology, Chinese Academy of Sciences, Qingdao, China; ¹²GEOMAR Helmholtz Centre for Ocean Research Kiel, Kiel, Germany; ¹³Department of Geosciences, University of Oslo, Oslo, Norway; ¹⁴International Ocean Discovery Program, Texas A&M University, College Station, TX, USA; ¹⁵Department of Arctic Geology, The University Centre in Svalbard, Svalbard, Norway; ¹⁶NIOZ Royal Netherlands Institute for Sea Research, Den Burg, Texel, Netherlands; ¹⁷Department of Earth, Atmosphere and Environment, Northern Illinois University, DeKalb, IL, USA; ¹⁸Department of Geological Sciences, New Mexico State University, Las Cruces, NM, USA; ¹⁹Department of Earth and Atmospheric Sciences, University of Nebraska, Lincoln, NE, USA; ²⁰Department of Geography and Environmental Science, Northumbria University, Newcastle Upon Tyne, UK; ²¹Department of Geosciences, Virginia Tech, Blacksburg, VA, USA; ²²School of Earth Sciences and the SFI Research Centre in Applied Geosciences, University College Dublin, Dublin, Ireland; ²³Department of Environment, Geology, and Natural Resources, Ball State University, Muncie, IN, USA; ²⁴Applied Structural Geology, Department of Earth Sciences, Indian Institute of Technology Kanpur, Kanpur, India; ²⁵Department of Marine and Coastal Sciences, Rutgers University, New Brunswick, NJ, USA

Contents of this file

Figures S1 to S11

Additional Supporting Information (Files uploaded separately)

Captions for Tables S1 to S7

Introduction

Data provided here includes supplemental figures as referenced in the main text and the references listed in the supplementary material. Additional supplemental tables are uploaded into a single, separate Excel file. These include all individual raw data analyses for each type of data collected for the study as well as the analytical error for any secondary standard materials.

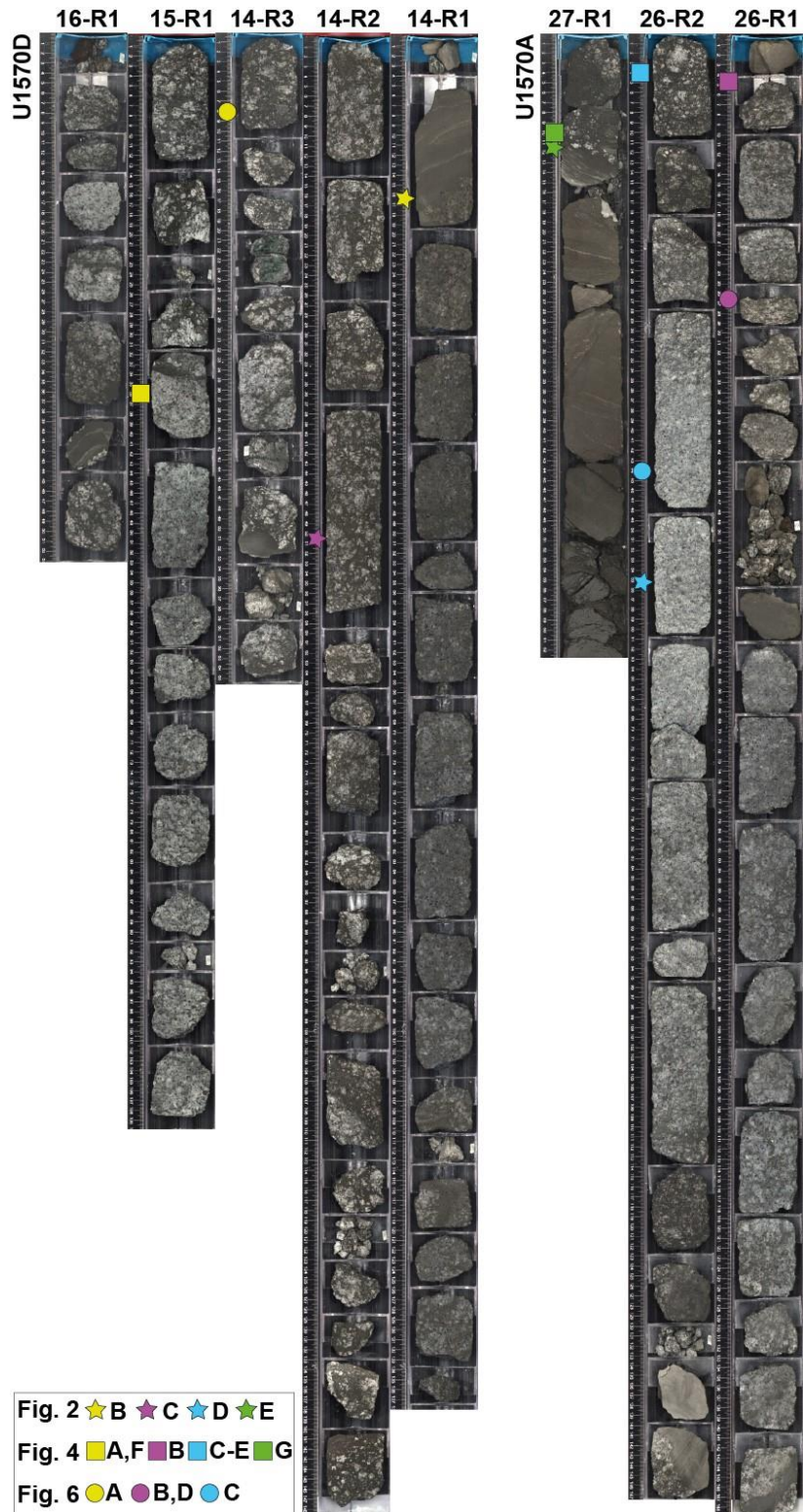


Figure S1. Core composite pictures of the dacite unit at holes U1570A and U1570D. The locations of the samples pictures provided in the main manuscript (Fig. 2: stars, Fig. 4: squares, and Fig. 6: circles) are shown with symbols.

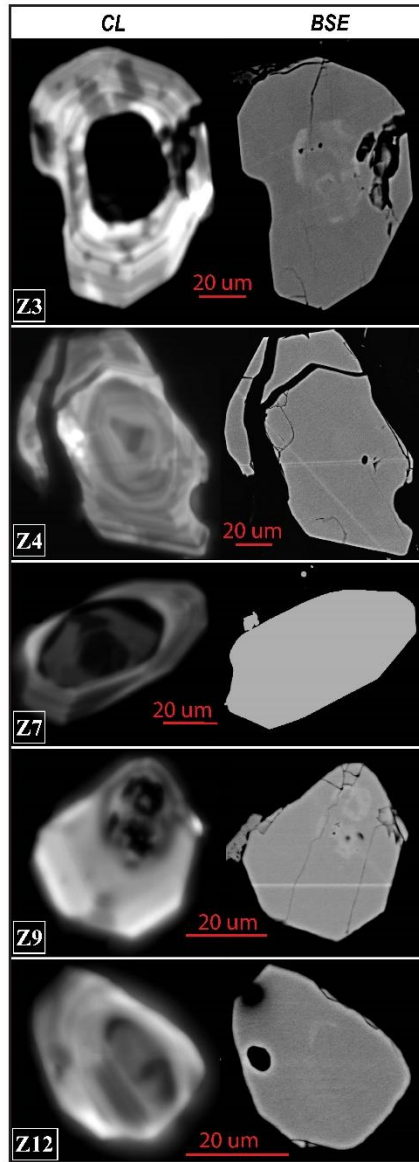


Figure S2. Cathodoluminescence (CL) and back-scattered electron (BSE) images of zircon grains presented in Fig. 10.

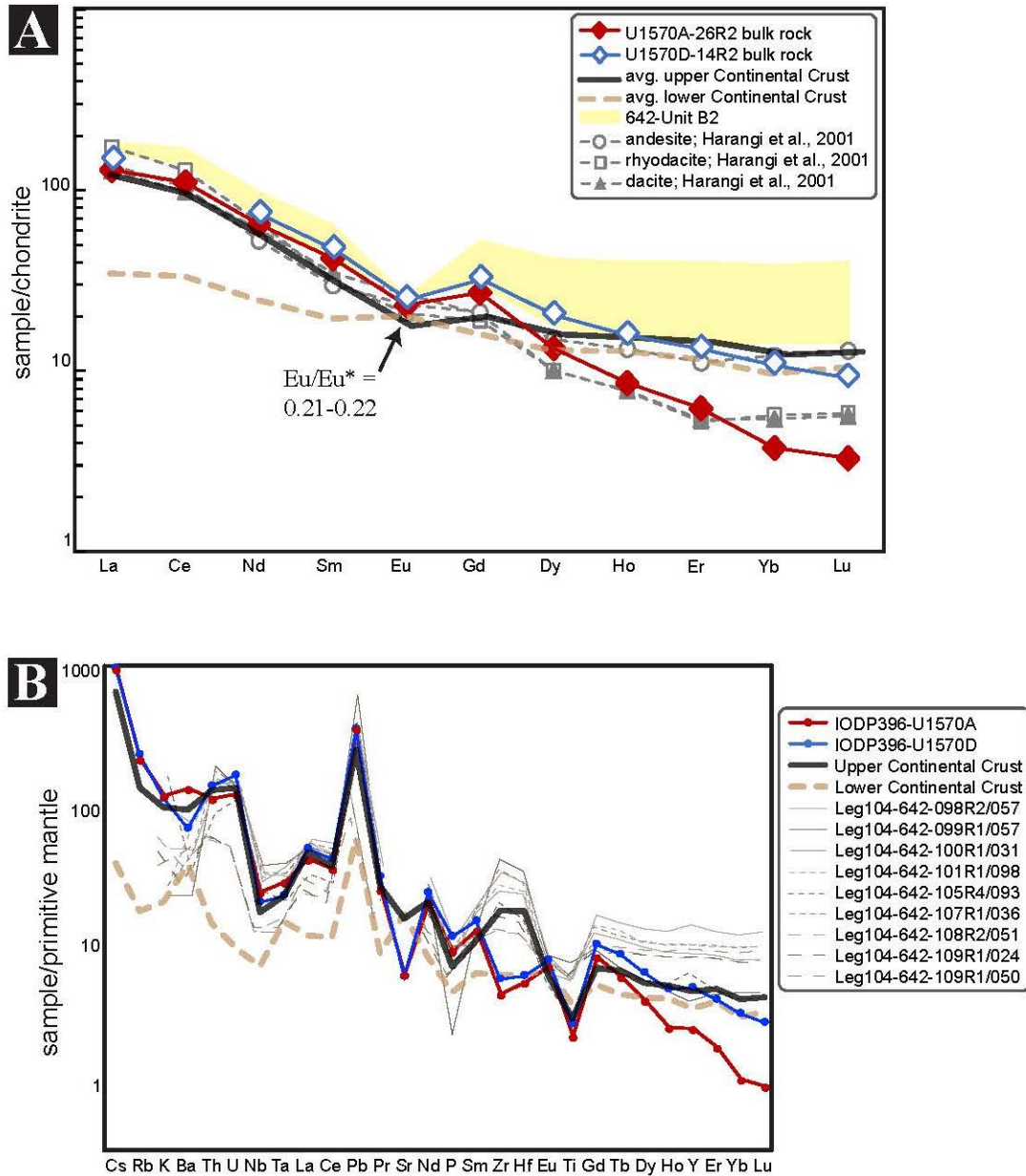
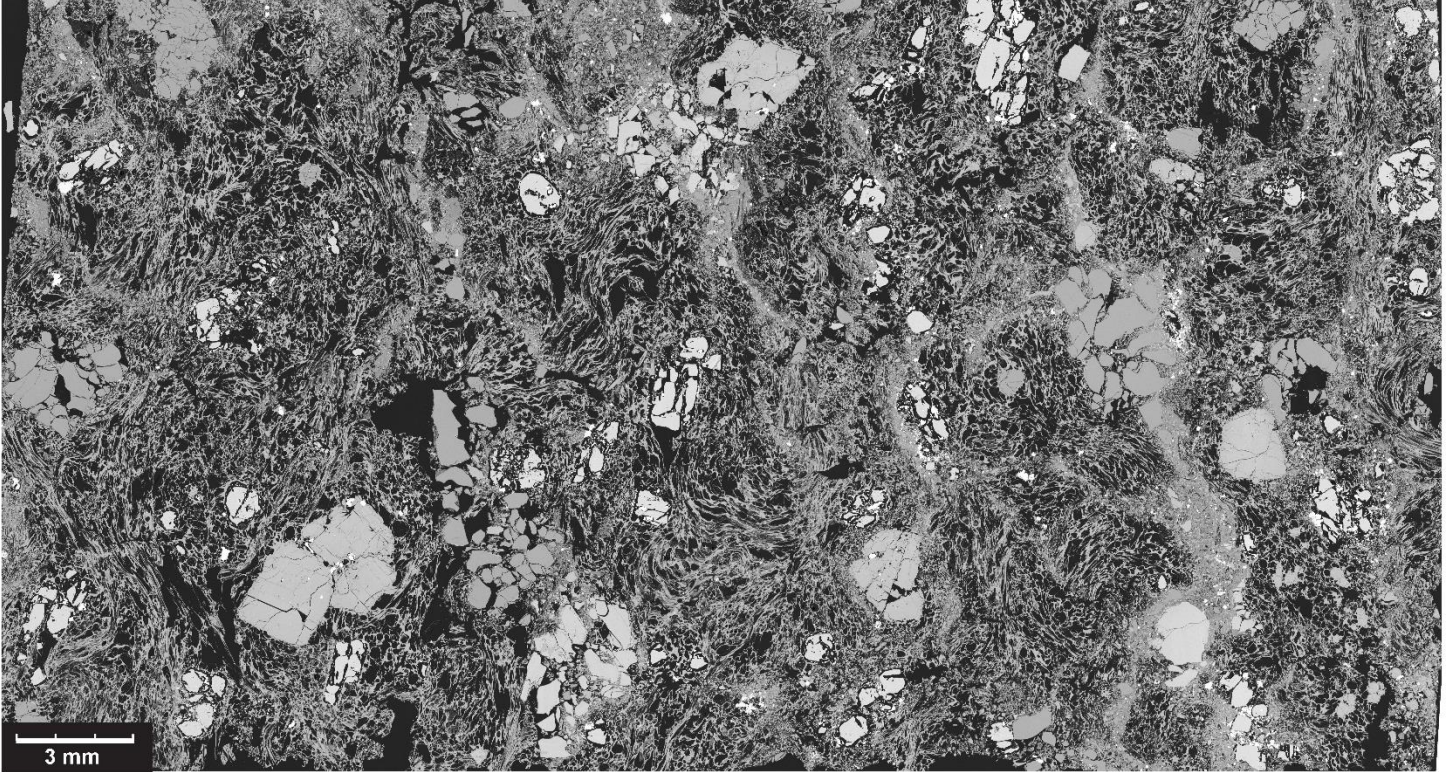
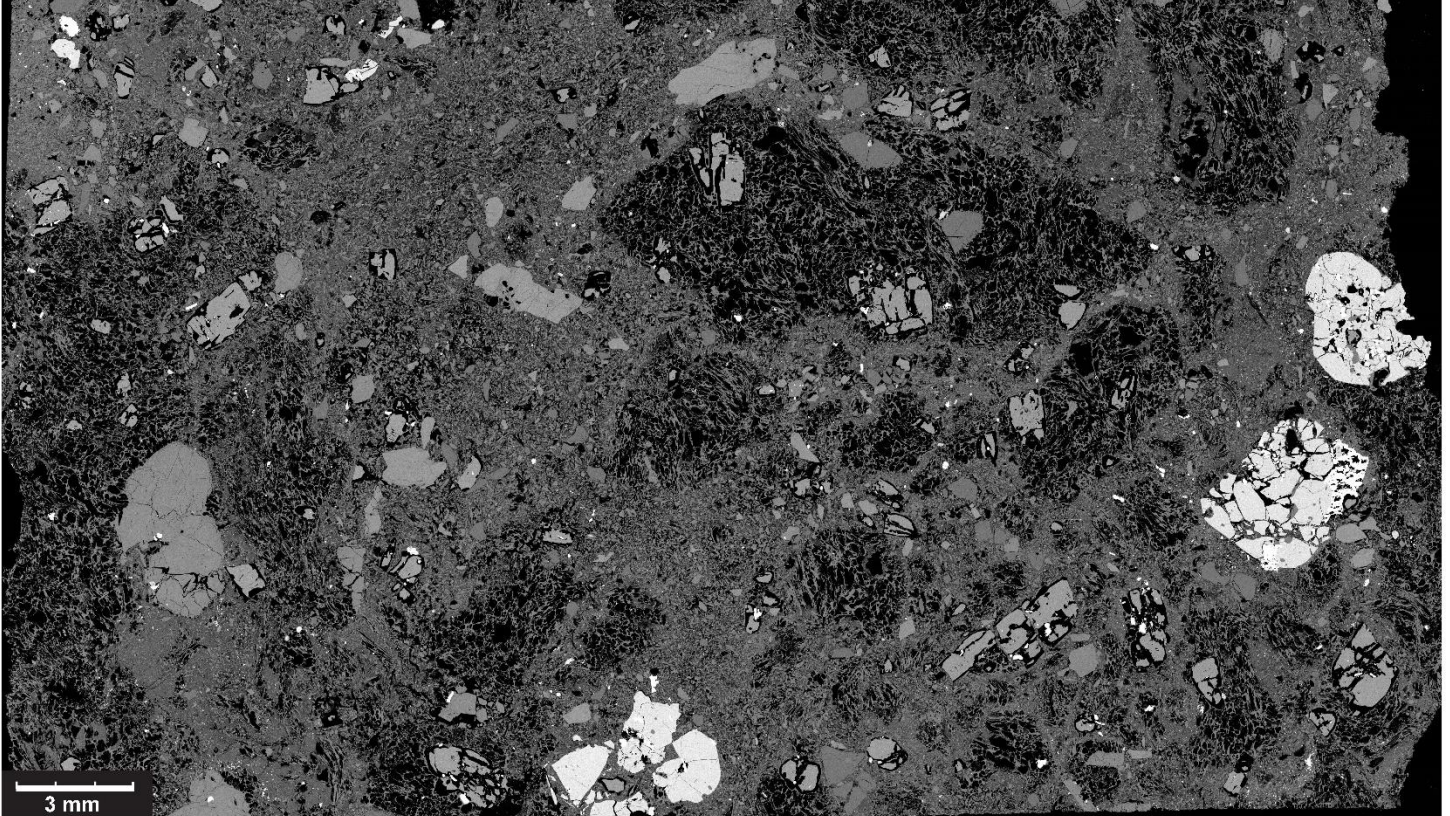


Figure S3. Chondrite-normalized (McDonough & Sun, 1995) bulk rock rare earth element (REE) concentrations for the two U1570 dacitic samples, compared with the average composition for the upper and lower continental crust (Rudnick & Gao, 2003), with the range of concentrations in Unit B2 for ODP 642E (yellow area, Meyer *et al.*, 2009a) and concentrations in calc-alkaline volcanic rocks from the Northern Pannonian Basin in Spain (gray symbols; Harangi *et al.*, 2001).

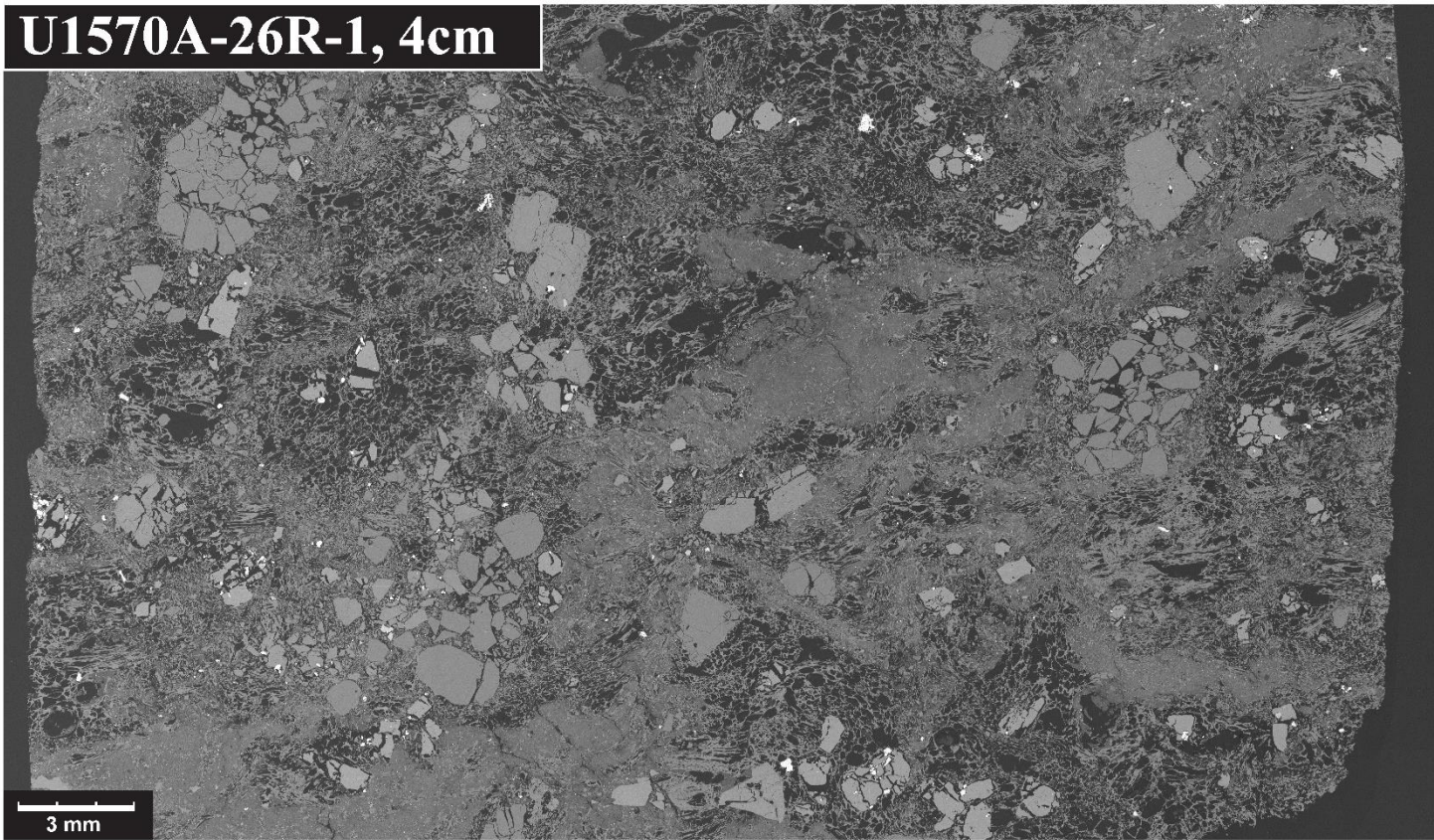
U1570D-15R-1, 36cm



U1570A-26R-2, 4cm



U1570A-26R-1, 4cm



U1570A-27R-1, 10cm

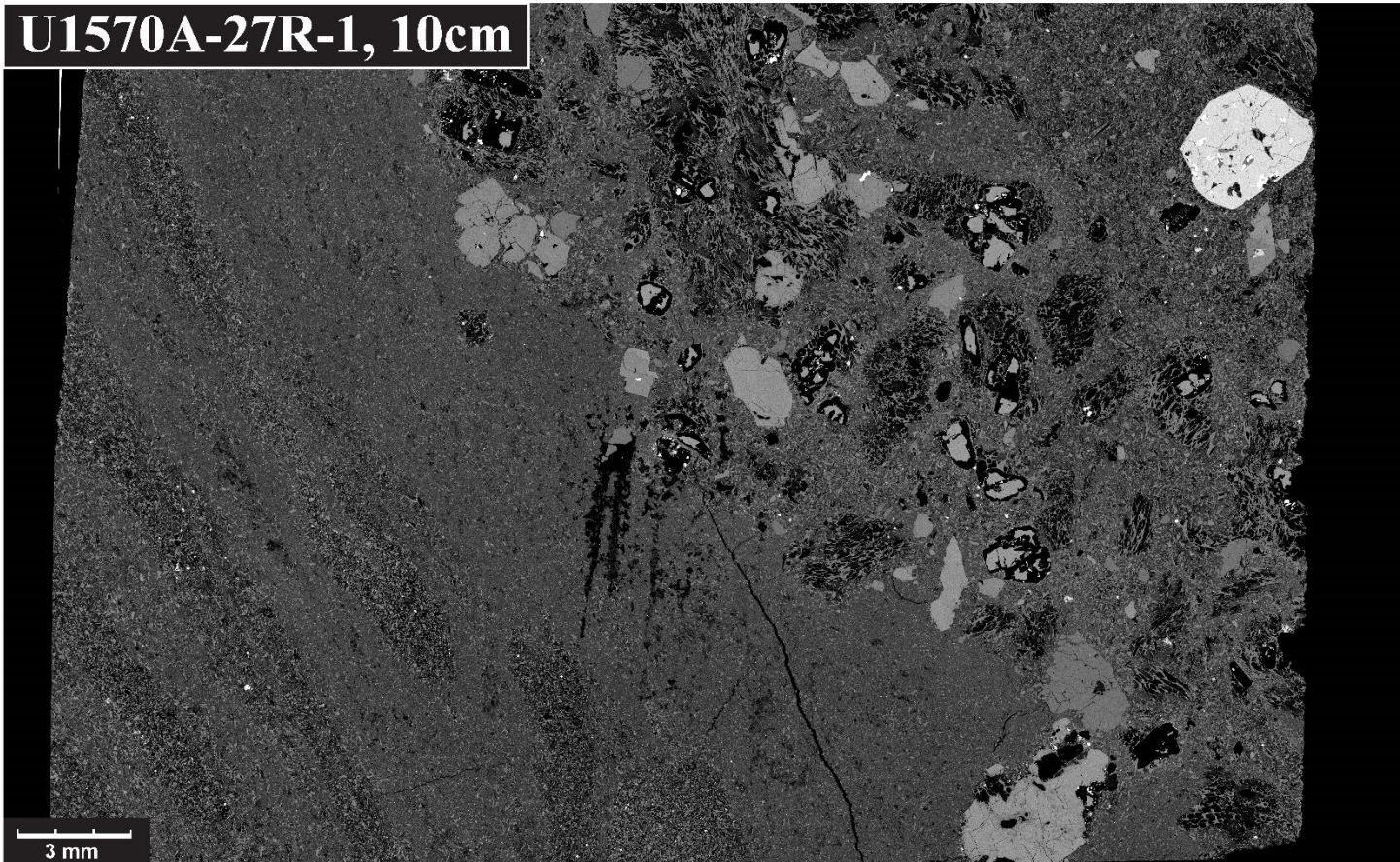


Figure S4. Full BSE maps of four thin sections of the Mimir dacite.

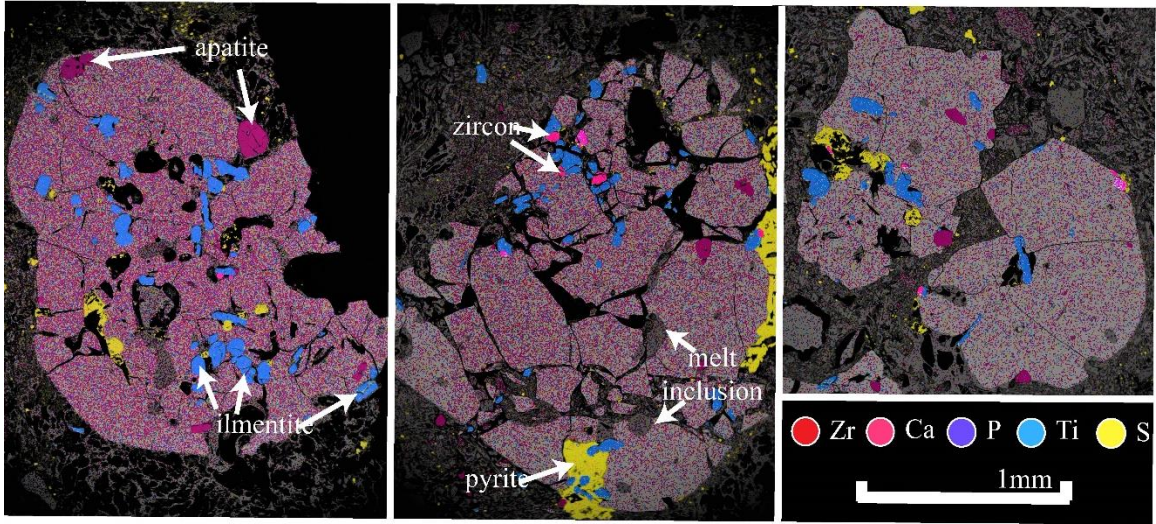


Figure S5. SEM-EDS maps of garnets from sample U1570A-26R2-4 showing the diversity of inclusions: ilmenite (blue), apatite (purple), zircon (bright pink), pyrite (yellow), and melt (dark gray). The scale bar is the same for all maps.

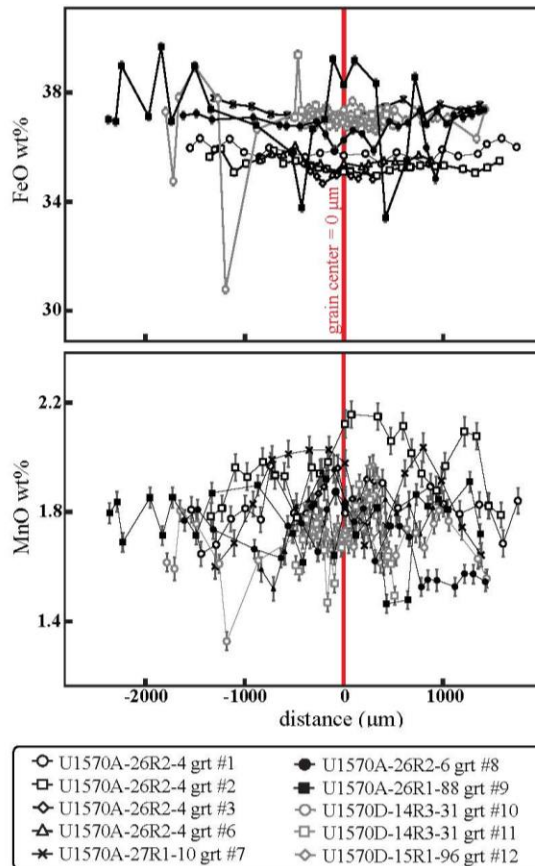


Figure S6. FeO (wt%) and MnO (wt%) profiles across garnet grains. Grain centers are represented by 0 μm red lines. Error bars represent the analytical uncertainty, 0.004 wt% and 0.03 wt%, respectively.

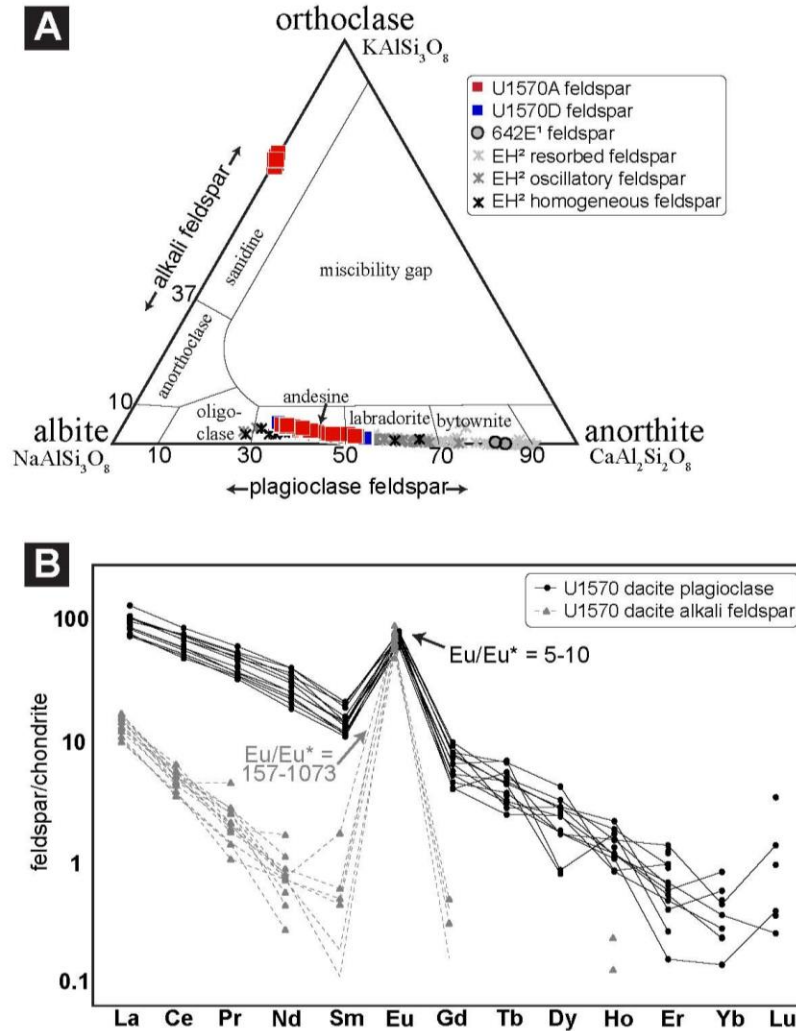


Figure S7. (A) Feldspar ternary classification diagram. Plotted are the alkali feldspar and plagioclase grains analyzed in the dacite samples from boreholes U1570A (red squares) and U1570D (blue squares) and plagioclase from 642E dacite (grey circles; Parson *et al.*, 1989). Data are compared with plagioclase from El Hoyazo (asterisks; Hiwatashi *et al.*, 2021) separated in three groups based on their texture: Resorbed and patchy (light grey), oscillatory zoning (dark grey) and homogeneous (black). (B) Chondrite-normalized (McDonough & Sun, 1995) feldspar REE concentrations. Plotted are plagioclase (black) and alkali feldspars (gray) from our samples.

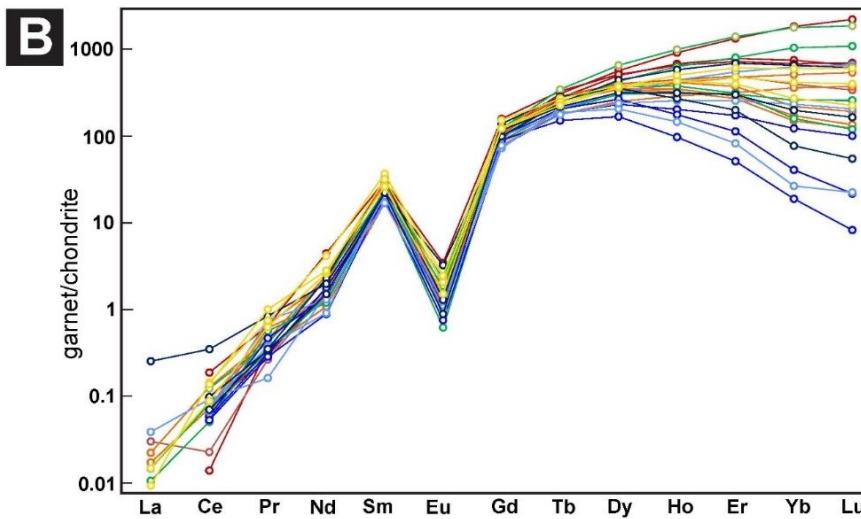
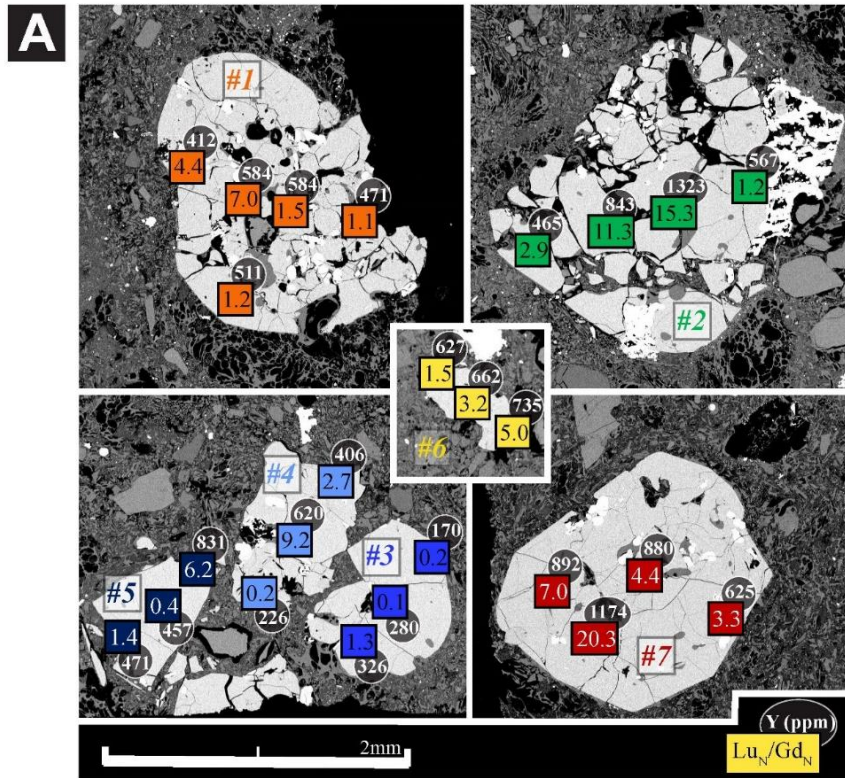


Figure S8. (A) SEM-BSE images of garnet grains analyzed by LA-ICP-MS. Garnets are numbered (from #1 to #7) according to how they are referred to in the text. Analysis locations are represented by colored squares; values on colored squares are the corresponding HREE slopes (i.e., Lu_N/Gd_N, chondrite-normalized ratio). Values in black circles are the Y (ppm) concentrations at the same location. Garnets #1, #2, #4 and #6 are all from the same sample (U1570A-26R2-4), while garnet #7 is from a sample near the base of the dacitic unit (U1570A-27R1-10). (B) Chondrite-normalized (McDonough & Sun, 1995) garnet REE concentration for each individual analysis performed on each of the seven garnets; colors correspond to those used in (A).

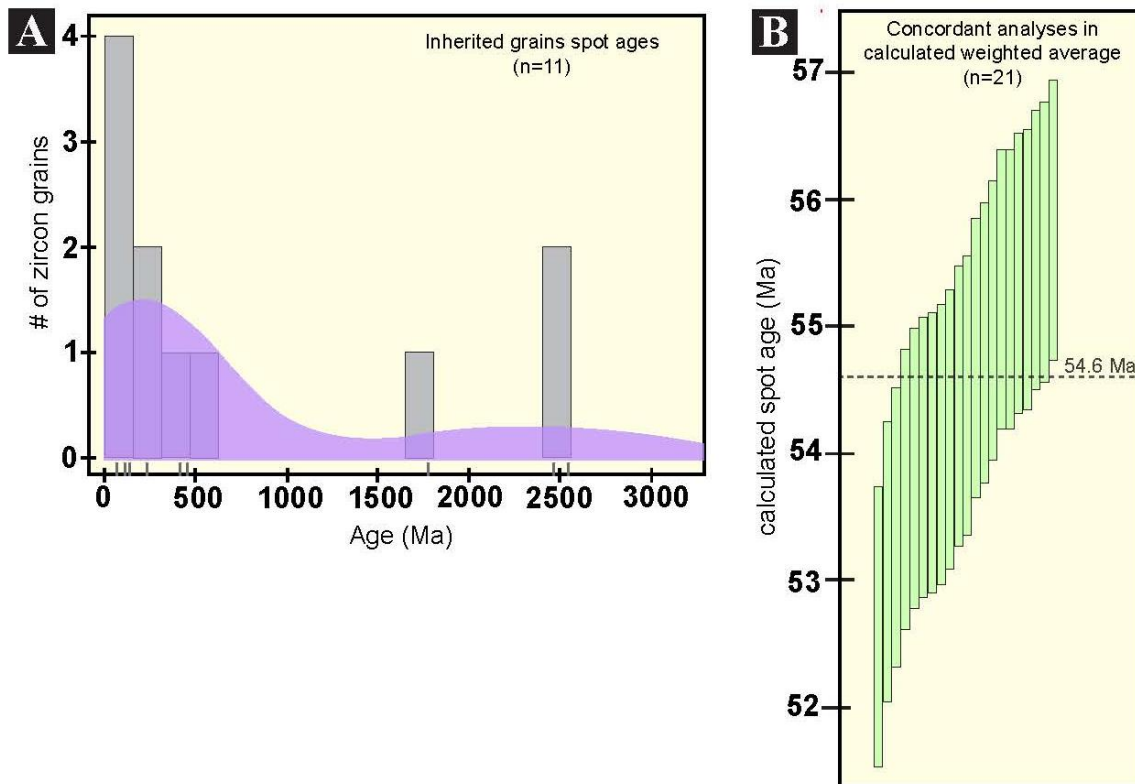


Figure S9. (A) Kernel density estimate (KDE) plot for the calculated spot ages of zircon grains in population #2 as defined by Fig. 10. (B) Calculated spot ages for young radiogenic, concordant analyses (population #1). The 54.6 Ma line represents the weighted mean for these analyses.

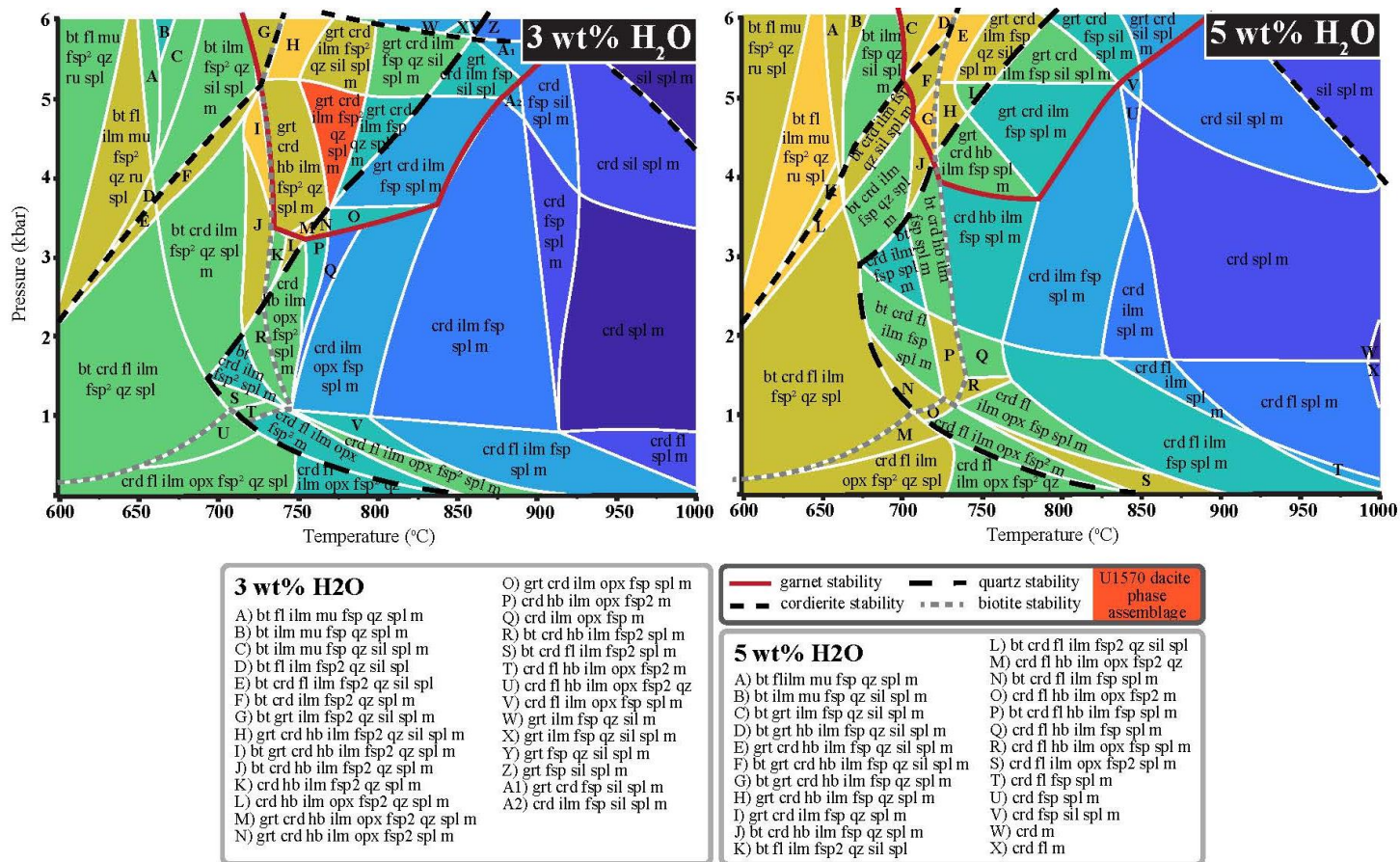


Figure S10. Pseudosections calculated with MAgEMin (Riel *et al.*, 2022) from the sample U1570-26R2-51-54 bulk rock composition of the dacite with 3wt % and 5 wt% H₂O contents. Colored fields ranging from blue to yellow represent an increasing number of phases in an assemblage; the dark orange field (H) represents the one that reproduced the observed assemblage in natural samples. Color code and abbreviations are the same as in Figure 6 in the main text.

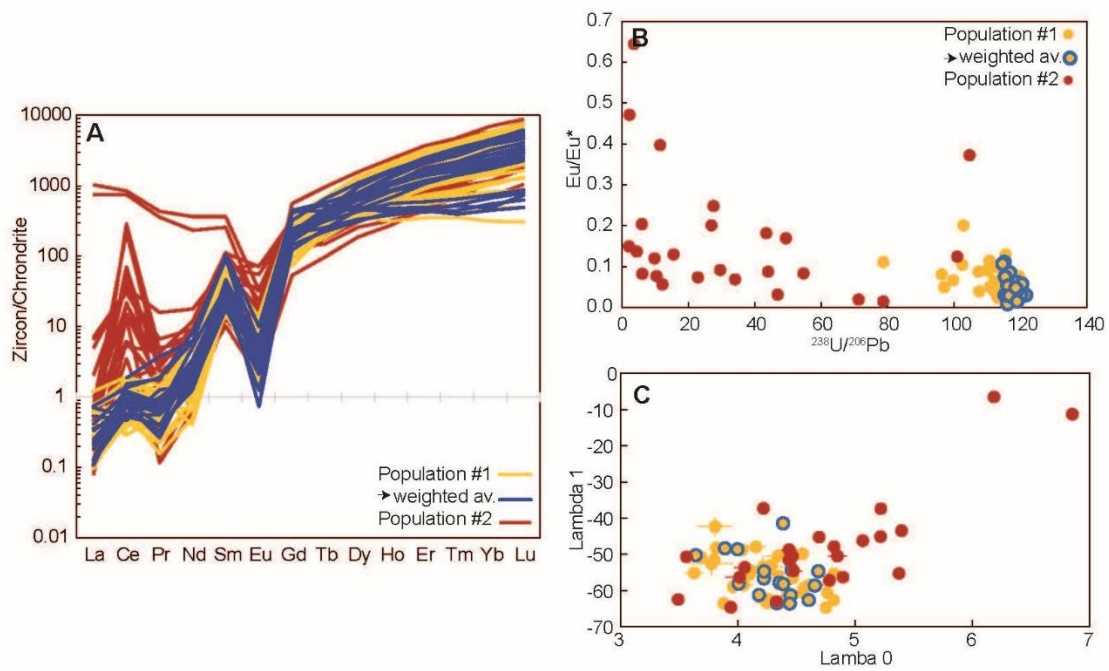


Figure S11. (A) Chondrite-normalized (McDonough & Sun, 1995) zircon REE concentration diagrams. (B) Eu anomalies (Eu/Eu^*) vs. $^{238}\text{U}/^{206}\text{Pb}$ ratio for zircon analyses. (C) Shape coefficients λ_0 and λ_1 for each analyzed zircon calculated using BLambdaR online software (Anenburg and Williams, 2022). Analyses for which La is below the limit of detection are excluded. Calculations were set up excluding Ce and Eu and without including tetrads in fitting. On each panel, populations #1 (including zircons used for the weighted average) and #2 are as defined in Figure 10.

Table S1. Composition, reproducibility and accuracy of the secondary standards during LA-ICP-MS and LASS analytical sessions.

Table S2. Dacite bulk concentrations.

Table S3. Major element oxide concentrations for individual analyses on major phases in the dacite.

Table S4. Trace element concentrations for individual analyses on major phases in the dacite.

Table S5. Carbon and nitrogen concentrations for sediments near the dacite.

Table S6. Hg concentration data for sediments near the dacite.

Table S7. Petrochronology data on zircons.

Supplementary References

- Anenburg, M., & Williams, M. J. (2022). Quantifying the tetrad effect, shape components, and Ce–Eu–Gd anomalies in rare earth element patterns. *Mathematical Geosciences*, 54(1), 47–70.
- Elhlou, S., Belousova, E., Griffin, W. L., Pearson, N. J., & O'Reilly, S. Y. (2006). Trace element and isotopic composition of GJ-red zircon standard by laser ablation. *Goldschmidt Conference Abstracts*, 1. doi:10.1016/j.gca.2006.06.1383
- Jochum, K. P., Nohl, U., Herwig, K., Lammel, E., Stoll, B., & Hofmann, A. W. (2005). GeoReM: A new geochemical database for reference materials and isotopic standards. *Geostandards and Geoanalytical Research*, 29, 333–338.
- Jochum, K. P., Weis, U., Stoll, B., Kuzmin, D., Yang, Q., Raczek, I., Jacob, D. E., Stracke, A., Birbaum, K., Frick, D. A., Günther, D., & Enzweiler, J. (2011). Determination of reference values for NIST SRM 610–617 glasses following ISO guidelines. *Geostandards and Geoanalytical Research*, 35(4), 397–429.
- Lambart, S., Hamilton, S., Lang, O. I. (2022). Compositional variability of San Carlos olivine. *Chemical Geology*, 605, 120968. <https://doi.org/10.1016/j.chemgeo.2022.120968>
- McDonough, W. F., & Sun, S. (1995). The composition of the Earth. *Chemical Geology*, 120, 223–253.
- Meyer, R., Hertogen, J., Pedersen, R. B., Viereck-Götte, L., & Abratis, M. (2009). Interaction of mantle derived melts with crust during the emplacement of the Vøring Plateau, N.E. Atlantic. *Marine Geology*, 261(1–4), 3–16. <https://doi.org/10.1016/j.margeo.2009.02.007>
- Parson, L., Viereck, L., Love, D., Gibson, I., Morton, A., & Hertogen, J. (1989). The petrology of the lower series volcanics, ODP Site 642. *Proceeding of the Ocean Drilling Program, Scientific Results*, 104, 419–428.
- Riel, N., Kaus, B. J. P., Green, E. C. R., & Berlie, N. (2022). MAGEMin, an Efficient Gibbs Energy Minimizer: Application to Igneous Systems. *Geochemistry, Geophysics, Geosystems*, 23(7). doi.org/10.1029/2022GC010427
- Rudnick, R. L., & Gao, S. (2003). Composition of the Continental Crust. *Treatise on Geochemistry*, 3, 1–64.
- Sláma, J., Košler, J., Condon, D. J., Crowley, J. L., Gerdes, A., Hanchar, J. M., Horstwood, M. S. A., Morris, G. A., Nasdala, L., Norberg, N., Schaltegger, U., Schoene, B., Tubrett, M. N., & Whitehouse, M. J. (2008). Plešovice zircon - A new natural reference material for U-Pb and Hf isotopic microanalysis. *Chemical Geology*, 249(1–2), 1–35. doi.org/10.1016/j.chemgeo.2007.11.005